

Article

Improved Extreme Learning Machine Based UWB Positioning for Mobile Robots with Signal Interference

Jun Ma ^{1,2}, Xuechao Duan ^{1,2,*}, Chen Shang ^{1,2}, Mengjiao Ma ^{1,2} and Dan Zhang ³ 

¹ Key Laboratory of Electronic Equipment Structure Design of Ministry of Education, Xidian University, Xi'an 710071, China; jma_2020@stu.xidian.edu.cn (J.M.); ccshang@stu.xidian.edu.cn (C.S.); 20041211803@stu.xidian.edu.cn (M.M.)

² Hangzhou Institute of Technology, Xidian University, Hangzhou 311200, China

³ Department of Mechanical Engineering, York University, Toronto, ON M3J 1P3, Canada; dzhang99@yorku.ca

* Correspondence: xchduan@xidian.edu.cn

Abstract: For the purpose of tackling ultra-wideband (UWB) indoor positioning with signal interference, a binary classifier for signal interference discrimination and positioning errors compensation model combining genetic algorithm (GA) and extreme learning machine (ELM) are put forward. Based on the distances between four anchors and the target which are calculated with time of flight (TOF) ranging technique, GA-ELM-based binary classifier for judging the existence of signal interference, and GA-ELM-based positioning errors compensation model are built up to compensate for the result of the preliminary evaluated positioning model. Finally, the datasets collected in the actual scenario are used for verification and analysis. The experimental results indicate that the root-mean-square error (RMSE) of positioning without signal interference is 14.5068 cm, which is reduced by 71.32% and 59.72% compared with those results free of compensation and optimization, respectively. Moreover, the RMSE of positioning with signal interference is 28.0861 cm, which is decreased by 64.38% and 70.16%, in comparison to their counterparts without compensation and optimization, respectively. Consequently, these calculated results of numerical examples lead to the conclusion that the proposed method displays its wide application, high precision and rapid convergence in improving the positioning accuracy for mobile robots.

Keywords: ultra-wideband (UWB); robot indoor positioning; genetic algorithm (GA); extreme learning machine (ELM); errors compensation



Citation: Ma, J.; Duan, X.; Shang, C.; Ma, M.; Zhang, D. Improved Extreme Learning Machine Based UWB Positioning for Mobile Robots with Signal Interference. *Machines* **2022**, *10*, 218. <https://doi.org/10.3390/machines10030218>

Academic Editor: Antonios Gasteratos

Received: 14 February 2022

Accepted: 15 March 2022

Published: 21 March 2022

Publisher's Note: MDPI stays neutral with regard to jurisdictional claims in published maps and institutional affiliations.



Copyright: © 2022 by the authors. Licensee MDPI, Basel, Switzerland. This article is an open access article distributed under the terms and conditions of the Creative Commons Attribution (CC BY) license (<https://creativecommons.org/licenses/by/4.0/>).

1. Introduction

The indoor positioning for mobile robots can hardly be realized by global positioning system (GPS) technology used mainly for outdoor positioning because GPS accuracy can degrade significantly in indoor scenarios [1–3]. Currently, several common optional technologies for indoor positioning of mobile robots have been proposed, including visible light communication (VLC) [4], Wi-Fi [5], magnetic patterns [6,7], radio frequency identification technology (RFID) [8], which can be used as potential alternatives to GPS. More importantly, localization using Wi-Fi and magnetic field does not necessitate the configuration of extra hardware. Although VLC and RFID are highly accurate, they are susceptible to interference from ambient light and objects containing metal, respectively. Zigbee, as another positioning technology, has been used in the indoor positioning of mobile robots with a precision of up to 0.636 m (in the range of 4 m × 4 m) [9]. Wireless local area network (WLAN) [10,11], also, has been utilized as a candidate solution for indoor localization, yet the location accuracy it offers needs to be improved. Weighing and considering the relationship between cost and accuracy, the original intention of this paper is to achieve higher positioning accuracy at a lower cost, even in signals being in strong interference.

Therefore, UWB positioning, a technology more suitable for indoor positioning, because of its advantages of high precision [12], low loss [13], collaborative localization [14,15],

resistance to harsh multipath effects [16,17] and more robustness to interference [18], is commonly extensively used in short-range wireless communications, such as in the field of mobile robots [19], aerial robotics [20], swarm and multi-robot systems [21], human-robot interaction [22,23], etc. With the widespread application of mobile robots in indoor scenarios [14], UWB positioning technology has become a pivotal method for indoor navigation and positioning, especially in indoor mobile transportation scenarios [24], such as urban canyons [25,26], hospitals [27] and IoT factories [14]. For instance, Lu et al. [28] proposed an assisted navigation system for blind and visually impaired persons utilizing a deep reinforcement learning guiding robot with UWB voice beacons and semantic feedback. Wu et al. [29] designed a UWB-based indoor food delivery robot location information system.

However, UWB positioning technology indoors will result in inaccurate positioning due to measurement errors caused by obstacles [30] and Non-Line-of-Sight (NLOS) [13,30]. To deal with the aforementioned problem, several techniques for improving UWB positioning accuracy have been previously proposed in recent decades. For example, Sandra et al. [31] introduced a unique approach that combines trilateration and fingerprinting to tackle the challenge of UWB-based localization in complicated indoor environments, which can reach sub-decimeter level precision. Considering the problem of locating a single robot given a set of squared noisy range difference (SRD-LS) measurements to a set of known-positions anchors, the work Pinar [32] performed regarding the localization errors has a probability of 90% within 0.35 m. Tiemann et al. [19] developed a technique for enhancing and integrating UWB with monocular simultaneous localization and mapping at 13.9 cm inaccuracy (6×6 m square at 4.5 m height). More so, a multi-sensor fusion localization method was proposed for improving the positioning accuracy and stability of mobile robots [33–38], but its implementation cost is too high [39]. Nevertheless, Liu et al. [40] fused the Inertial-measurement unit (IMU) and UWB with a particle filter to obtain a position error of 0.534 m. A UWB and improved pedestrian dead-reckoning (PDR) integration algorithm has been applied to dynamic indoor positioning [41], but it can only provide the positioning accuracy of approximately 51 cm in a two-dimensional scene. The particle filter solution proposed by Guido et al. [42] has slightly better performance but at the price of increased computational complexity. Likewise, an indoor positioning optimization algorithm combining GA and radial basis function (RBF) neural network (GA-RBF) was proposed by Guo et al. [43], whose positioning error is within 10 cm only in a two-dimensional plane. In addition, Guo et al. [44] proposed another method that the optimized neural network clustering algorithm is integrated with the unscented Kalman filter (UKF) to smooth the positioning data and reduce NLOS error. Besides, deep learning-based localization, for UWB systems was proposed by Nguyen et al. [45] that utilizes a convolutional neural network (CNN), for GPS in mobile robots, was adopted by Nilwong et al. [46]. Similarly, machine learning-based algorithms were developed by Rana et al. [47] through multi-class support vector machine (MC-SVM) architecture enabling a truly evolving scheme to both localize targets and identify them in a useful way. Schmid et al. [16] have used a part of the large dataset to train an artificial neural network (ANN) for errors prediction; mean absolute bias along the bench was about 8 cm, and the average standard deviation per position was only 4 cm, however, at specific locations mean errors were over 60 cm. An anchor placement method for the trajectory of target based on genetic heuristic differential evolution algorithm was proposed by Pan et al. [48] that its average localization error is 0.56 m.

In summary, there are a multitude of methods towards improving the accuracy of UWB indoor positioning, among which the accuracy of fusion of multiple sensors with high costs is proved to be optimal. If only UWB positioning technology is used, owing to low costs, centimeter-level accuracy can be achieved in a two-dimensional plane, whereas the accuracy it offers in a three-dimensional space is still underdeveloped. Furthermore, little literature has investigated the problem of UWB signals being in strong interference, i.e., abnormal data fluctuations usually caused by time delay will cause indoor positioning to be inaccurate. Therefore, the precise positioning of UWB in signal interference (e.g., obscuration between anchors and target) is regarded as an urgent problem to be solved. In

this paper, a UWB indoor high-precision positioning model based on GA-optimized ELM is proposed, as a component of which, a binary classifier based on GA-ELM is established to judge the existence of signal interference, and the positioning errors compensation is then performed by using the GA-ELM model to realize the precise positioning of the mobile robot target in complex indoor environments.

2. Preliminary Positioning and Assessment Model

The UWB positioning anchor receives data packets with less interference, so hundreds to thousands of positioning tags can work in the same area at the same time. Concerning the influence of the number of anchors, it is necessary to discuss first. Theoretically, the more the number of positioning base stations, the higher the positioning accuracy of the target to be measured, but there is a lower limit to the number of base stations. Since the equation expressing the distance between the target and the anchors contains quadratic terms, at least $N_p + 1$ sets of equations are required to solve the N_p -dimensional quadratic equations, i.e., the number of anchors N_B and unknown quantities in the set of equations, and also the spatial dimension must satisfy the following equation:

$$N_B \geq N_p + 1 \quad (1)$$

Equation (1) shows that indoor three-dimensional spatial positioning requires four or more base stations, so four anchors are chosen to be adopted in this paper.

In the actual scene, the TOF ranging principle, a technique that uses the time of flight of radio waves between two objects to calculate distance, is first used to acquire the distances between the four anchors that transmit the signals and the target that receives the signals. The schematic diagram of the experimental scene, as well as the operational principle of data collection, are shown in Figure 1. In particular, the position coordinates of the four anchors are fixed at different heights indoors, while the mobile robot with the target (i.e., Tag in Figure 1) moves in the indoor environment, and the four anchors and the target sense each other through UWB pulses. Each movement of the target can be recorded with the information occurring in these four-communication links consisting of four anchors and the target. Through the mutual communication between the four anchors and the target, the spatial distance between each pair is accordingly measured with TOF technology.

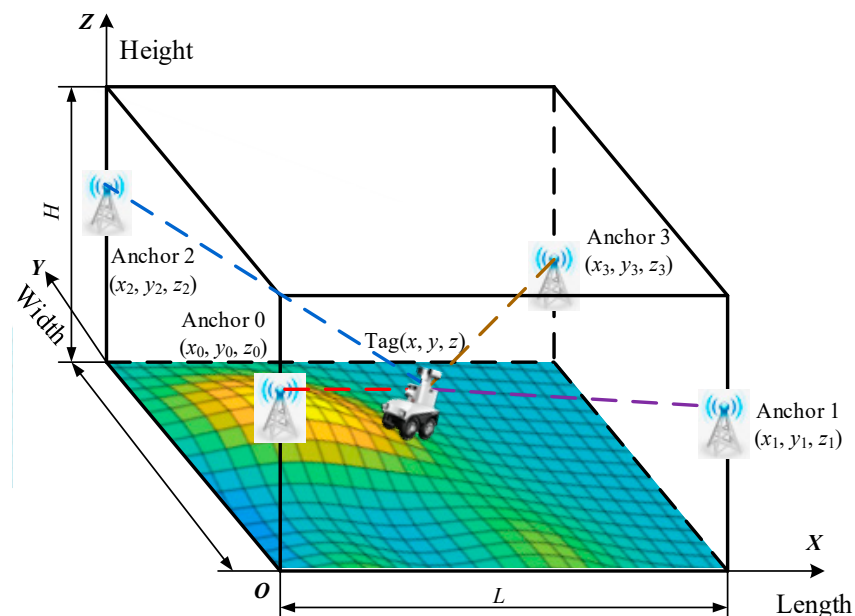


Figure 1. Schematic diagram of the principle of TOF-based UWB data collection.

Next, according to the collected ranging dataset of the target, a preliminary positioning mathematical model is established to initially calculate the three-dimensional coordinates of the target by following these detailed steps:

Step 1: The distance \bar{D}_{A_t} (obtained by TOF ranging) between the target and anchor t is denoted as

$$\bar{D}_{A_t} = \sqrt{(x_t - x)^2 + (y_t - y)^2 + (z_t - z)^2}, t = 0, 1, 2, 3. \quad (2)$$

Step 2: Squaring both sides of Equation (2) lead to

$$\begin{cases} \bar{D}_{A_0}^2 = x_0^2 + y_0^2 + z_0^2 - 2x_0x - 2y_0y - 2z_0z + x^2 + y^2 + z^2, \\ \bar{D}_{A_1}^2 = x_1^2 + y_1^2 + z_1^2 - 2x_1x - 2y_1y - 2z_1z + x^2 + y^2 + z^2, \\ \bar{D}_{A_2}^2 = x_2^2 + y_2^2 + z_2^2 - 2x_2x - 2y_2y - 2z_2z + x^2 + y^2 + z^2, \\ \bar{D}_{A_3}^2 = x_3^2 + y_3^2 + z_3^2 - 2x_3x - 2y_3y - 2z_3z + x^2 + y^2 + z^2. \end{cases} \quad (3)$$

by the definition simultaneously:

$$H_t = x_t^2 + y_t^2 + z_t^2 \quad (4)$$

Step 3: The two adjacent terms of Equation (3) are subtracted to eliminate the quadratic term, hence, the target position $\text{Tag}(x, y, z)$ in matrix form is:

$$\begin{bmatrix} x \\ y \\ z \end{bmatrix} = \frac{1}{2} \begin{bmatrix} x_1 - x_0 & y_1 - y_0 & z_1 - z_0 \\ x_2 - x_1 & y_2 - y_1 & z_2 - z_1 \\ x_3 - x_2 & y_3 - y_2 & z_3 - z_2 \end{bmatrix}^{-1} \begin{bmatrix} \bar{D}_{A_0}^2 - \bar{D}_{A_1}^2 + H_1 - H_0 \\ \bar{D}_{A_1}^2 - \bar{D}_{A_2}^2 + H_2 - H_1 \\ \bar{D}_{A_2}^2 - \bar{D}_{A_3}^2 + H_3 - H_2 \end{bmatrix} \quad (5)$$

Step 4: The RMSE, which is used for evaluating the positioning model accuracy of the mobile robot, is calculated as:

$$RMSE_j = \sqrt{\frac{1}{n} \sum_{i=1}^n (y_i - \hat{y}_i)^2}, j \in \{X, Y, Z\} \quad (6)$$

where $RMSE_j$ represents the root-mean-square error of the coordinates y_i and \hat{y}_i are the true value and estimated value of the i -th target coordinate, respectively.

Step 5: The degree of the fitting test is used to verify the fitting degree of the prediction model to the sample observations value. The sum of squares of the mean difference between the original and predicted data is given by:

$$S_t = \sum_{i=1}^n (y_i - \bar{y})^2 = \sum_{i=1}^n (y_i - \hat{y})^2 + \sum_{i=1}^n (\hat{y} - \bar{y})^2 = S_c + S_h \quad (7)$$

As a satisfactory prediction model, the sample observation values should be well fitted, i.e., S_c in S_t should be as small as possible, so the degree of fitting can be defined as:

$$R^2 = 1 - \frac{S_c}{S_t} \quad (8)$$

The closer R^2 is to 1, the stronger the explanatory ability of the independent variable of the analytical formula to the dependent variable, which means that there is a better fitting effect of the equation and a higher fitting degree of the data.

3. Precise Positioning Model

In this section, the details of the UWB-based precise positioning model for mobile robots proposed in this paper are illustrated as follows. First, the general framework of the method proposed in this contribution is presented. Afterward, the ELM model is established, followed by the GA-optimized ELM model is constructed for improving the positioning accuracy of mobile robots.

3.1. Construction of Overall Model

No matter whether the signal interference exists, accurate positioning (three-dimensional coordinates) of the target can be obtained by the GA-optimized ELM model for positioning errors compensation and its specific process is shown in Figure 2.

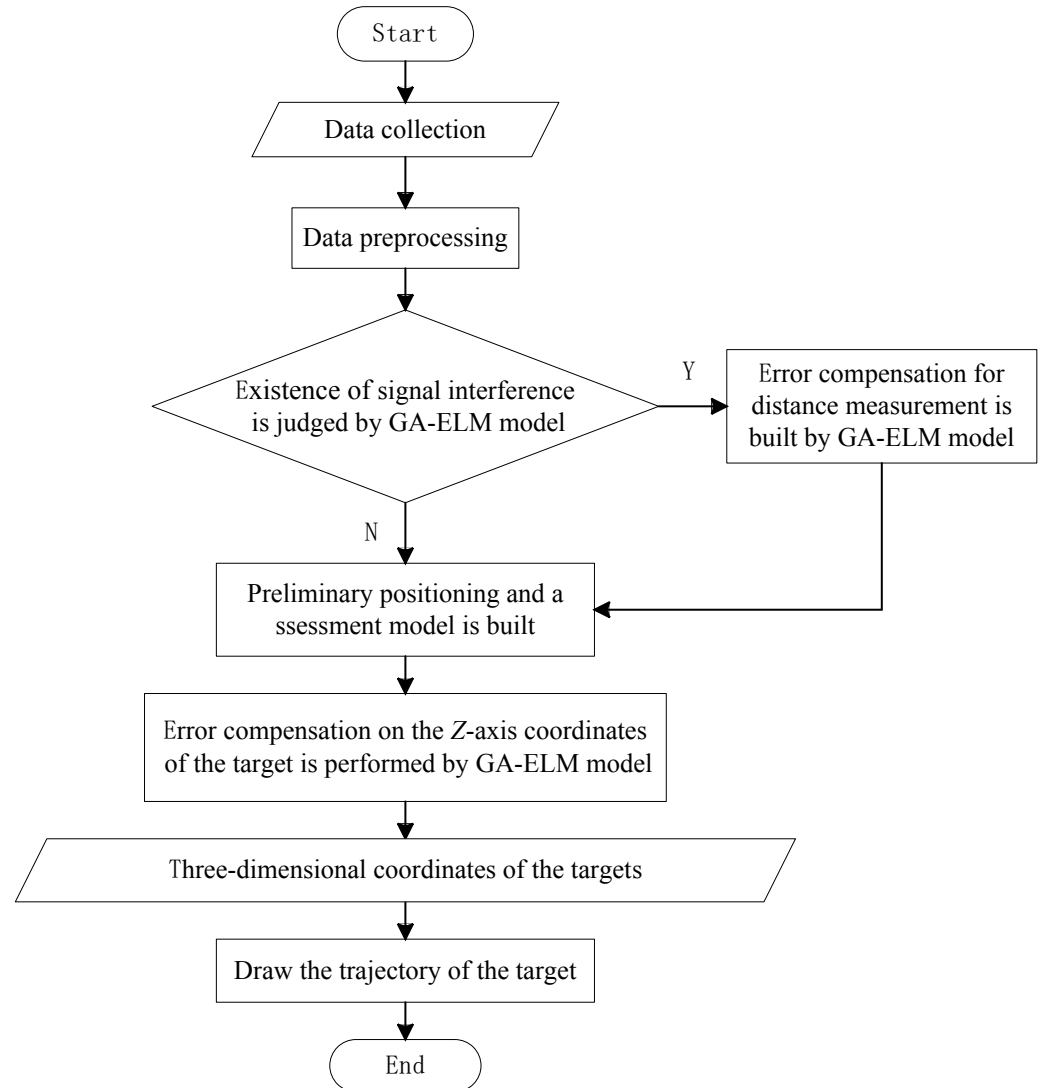


Figure 2. Workflow chart of the overall method.

It is worthwhile mentioning, in the workflow of the overall method proposed in this paper, that the GA-optimized ELM model is adopted three times, in which signal discrimination, Z-axis errors compensation and ranging errors compensation, respectively, embodies the reusability of the same method regarding the GA-ELM model.

3.2. Construction of the ELM Model

Compared with traditional training methods (e.g., BP neural network), ELM has the advantages of higher learning speed and better generalization performance [49]. In addition, ELM can not only predict the positioning errors of the target but also judge whether signal interference exists during the positioning process of the mobile robot using UWB technology.

In this research, the ELM model is established to train the nonlinear relationship between ranging data (between targets and anchors) and category or error, as shown in Figure 3. The input variable x is actual ranging data, and the output variable t is error or category. The input layer, hidden layer and output layer has n , l and m neurons, respectively.

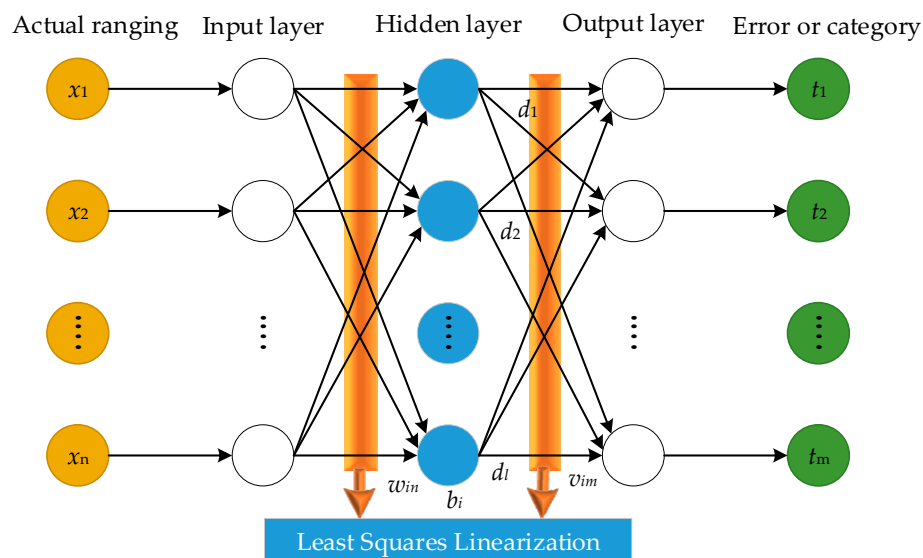


Figure 3. The network topological structure diagram of ELM based on least squares linearization.

Suppose there are N groups of training samples for ranging, between four anchors (A_0, A_1, A_2, A_3) and the target, is $(x_i, t_i) \in \mathbf{R}^n \times \mathbf{R}^m$. Subsequently, the ELM model can be expressed as:

$$O_k = \sum_{i=1}^l v_i g(w_i x_k + b_i), k = 1, 2, \dots, N \tag{9}$$

where $g(x)$ is the excitation function, $w_i = [w_{i1}, w_{i2}, \dots, w_{in}]^T$ is the weight coefficient of the connection between the i -th node of the hidden layer and the input layer, $v_i = [v_{i1}, v_{i2}, \dots, v_{im}]^T$ is the weight coefficient of the connection between the i -th node of the hidden layer and the output layer, and b_i is the threshold of hidden layer nodes.

In the case of $l = N$, Equation (9) is defined as:

$$Hv = T \tag{10}$$

where

$$\begin{cases} H = \begin{bmatrix} g(w_1 x_1 + b_1) & \dots & g(w_l x_1 + b_l) \\ \vdots & & \vdots \\ g(w_1 x_N + b_1) & \dots & g(w_l x_N + b_l) \end{bmatrix}_{N \times l}, \\ v = [v_1^T, \dots, v_l^T]_{l \times m}^T, \\ T = [t_1^T, \dots, t_l^T]_{N \times m}^T. \end{cases}$$

If the number of datasets is large, $l < N$ is taken to reduce the computation, and the network model of ELM is calculated as:

$$\min \|Hv - T\| \tag{11}$$

where $g(x)$ is infinitely differentiable, the weight coefficient w_i and the threshold b_i are all random numbers limited in the interval $[-0.5, 0.5]$, and the training process of the ELM can be regarded as solving the least square solution of the linear system $Hv = T$, namely:

$$\hat{v} = H^+ T \tag{12}$$

where H^+ is the Moore–Penrose generalized inverse matrix of H .

Eventually, substituting the results of w , v and b into Equation (9) yield the result of the output layer.

3.3. Construction of GA-Optimized ELM Model

Since the weight coefficients and thresholds of ELM are generated by random numbers, which leads to the prediction results of the model not being accurate enough, an optimization algorithm should be used to obtain the optimal value of weight coefficients and thresholds. Similarly, GA simulates the biological evolution process in nature rather than the traditional search method and employs the evolution method to perform a random optimization search on the target. In view of its global search optimal ability [50], this paper adopts GA to optimize the weight coefficients and thresholds of ELM, which effectively improves the positioning accuracy of the target and the correct rate of judging the presence and absence of signal interference.

According to the input and output parameters of ELM, the number of GA optimization parameters is determined, so as to set the code length of population individuals. In the following, the fitness function adopts a linearly ordered fitness distribution function, which is defined as:

$$F(\rho) = 2 - \eta_{\max} + 2(\eta_{\max} - 1) \frac{\rho - 1}{\chi - 1}, \eta_{\max} \in [1, 2] \quad (13)$$

where ρ is the individual serial number, χ expresses the population size of the objective function value, η_{\max} indicates the selective pressure.

The selection operator uses random traversal sampling, the crossover operator uses single-point crossover, and the mutation operator generates the number of variant genes with a certain probability (i.e., change code 1 to 0 or change code 0 to 1).

The objective function of signal interference identification is to minimize the error rate, specifically:

$$\min_{w_i, v_i, b_i} \arg \mathfrak{R} = \left(1 - \frac{n_t}{N_t}\right) \times 100\% \quad (14)$$

where n_t and N_t represent the correct number and the total number of the test sets respectively, respectively.

The objective function of the target coordinate errors compensation is to minimize RMSE, specifically:

$$\min_{w_i, v_i, b_i} \arg \text{RMSE} = \sqrt{\frac{\|\varepsilon_c - \varepsilon_r\|_2^2}{N}} \quad (15)$$

where ε_c and ε_r mean the error prediction value and the true value of the test set, respectively.

Combining the advantages of GA and ELM, GA-optimized ELM based signal interference discrimination and positioning errors compensation algorithms are established, whose workflow chart is shown in Figure 4.

In this model, the weight coefficients and thresholds of ELM are optimized by GA to derive the optimal objective function value, which is used for the discrimination of signal interference and the positioning errors compensation with and without signal interference in mobile robots' positioning.

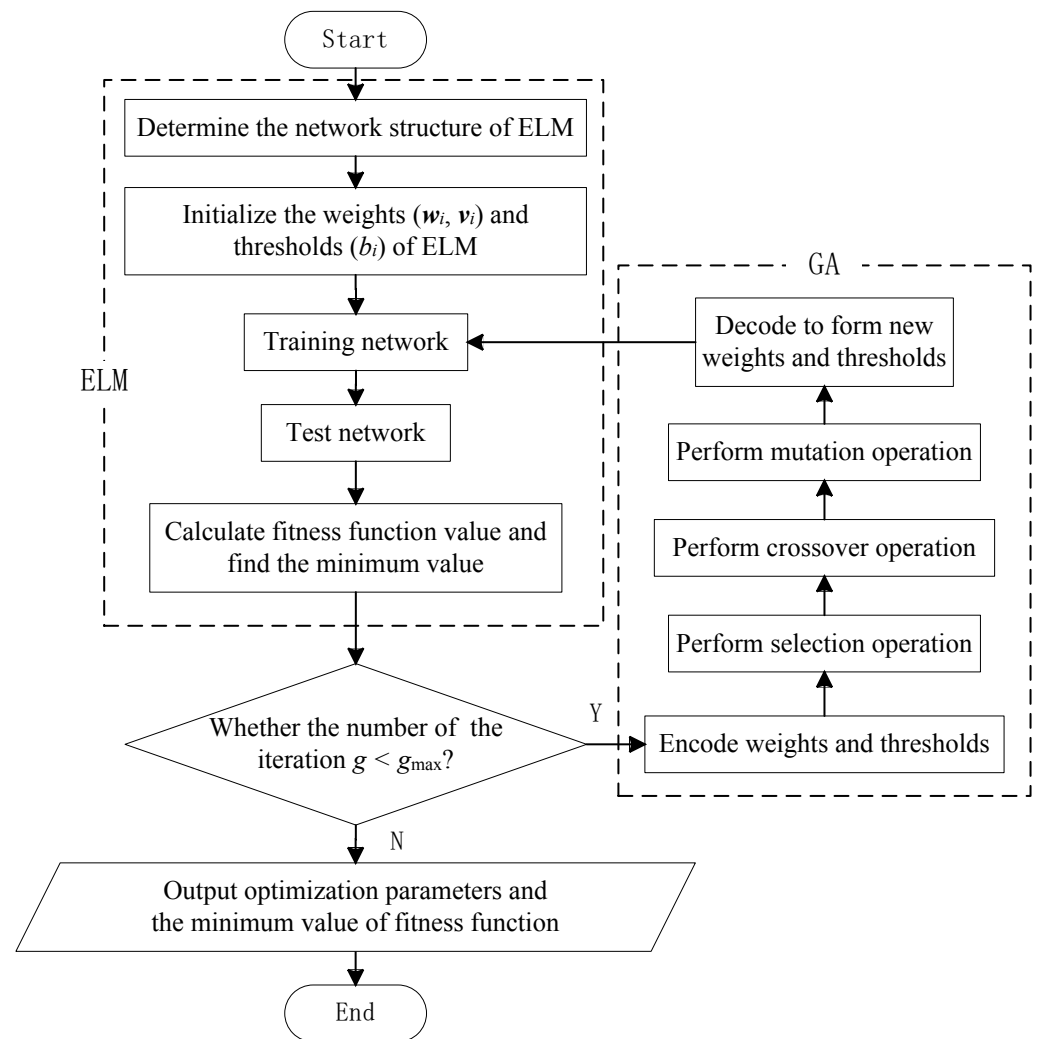


Figure 4. Workflow chart of GA-ELM algorithm.

4. Experimental Results and Analysis

In this section, measured experiments and analyses are carried out to obtain the evaluation results of the model proposed in Section 3. Data preprocessing is firstly performed to gain reliable and available datasets about the position of the target on the mobile robot, and then 324 datasets with and without signal interference, i.e., corresponding to two scenarios of NLOS and LOS, respectively, are tested and analyzed on the signal discrimination and the positioning errors compensation model proposed in this work.

4.1. Experimental Apparatus

The experiment is conducted in an indoor environment with a length, width and height of 5 m, 5 m and 3 m, respectively, specifically in Figure 1, $L = 5000$ mm, $W = 5000$ mm, $H = 3000$ mm, and the coordinates of the four anchors are $A_0(0, 0, 1300)$, $A_1(5000, 0, 1700)$, $A_2(0, 5000, 1700)$, $A_3(5000, 5000, 1300)$, respectively. The four anchors are arranged with different height differences to eliminate the Z-axis error.

In this experiment, a high-precision positioning base station (four anchors) and target with model DWM1000 UWB transceivers from Decawave are adopted to verify GA-ELM experimentally, which uses coherent receiving technology to enable the positioning system to realize object positioning, as well as has the advantages of low power consumption and high positioning accuracy. The basic parameters of Decawave-DWM1000 are shown in Table 1.

Table 1. Basic parameters of the base station and target.

	Model	Decawave-DWM1000
Power Supply	DC power	The input voltage is 2.8~3.6 V
UWB Wireless Parameters	Supported protocols	IEEE802.15.4-2011 UWB protocol
	Frequency	3.5 GHz~6.5 GHz
	The rate of data transfer	Support 6.8 Mbps, 110 kbps and 850 kbps
Positioning Performance	Positioning accuracy	<30 cm (No occlusion)
	Recommended base station layout interval	<300 m
	Supported ranging schemes	TOF and TDOA

4.2. Data Preprocessing

In the experimental scenario mentioned above, the UWB ranging data of the target at 324 different positions with and without signal interference were collected, respectively, that is, two datasets of data were collected for each position with and without signal interference, respectively, and the ranging of each group of the target at the identical position was collected multiple times to obtain the arithmetic mean for avoiding random errors of the measurement system.

Typically, in the process of data measurement, regardless of the presence and absence of signal interference, the measured value may be affected by the environment, resulting in deviations in the measurement data, i.e., abnormal values, which will interfere with subsequent model predictions. Correspondingly, according to the number of measurements, 3σ criterion is selected for performing data processing to obtain usable data, whose calculation process is as follows.

Step 1: The mean value of the ranging samples is calculated to mitigate systematic random errors as follows:

$$\bar{d} = \frac{1}{n} \sum_{i=1}^n d_i \quad (16)$$

where n represents the number of samples, d_i is the distance measurement between the target and anchors in the i -th sample.

Step 2: Sample standard deviation S is obtained by:

$$S = \sqrt{\frac{1}{n} \sum_{i=1}^n (d_i - \bar{d})^2} \quad (17)$$

If the residual error of the measured value d_m satisfies $|d_m - \bar{d}| > 3\sigma$, it is considered as an abnormal value that must be eliminated.

As mentioned above, the standard deviation comparison of each location ranging datasets without and with signal interference before and after processing is shown in Figures 5 and 6, respectively.

From the comparison of Figures 5 and 6, it can be directly seen that the standard deviation after data preprocessing has been reduced, especially for anchors A_0 and A_3 , indicating that the selected approach is correct and effective. The most remarkable result is that the standard deviation of the datasets is large in the case of signal interference, illustrating that there are numerous abnormal values in the measured datasets in the condition of signal interference, which can effectively verify the effectiveness and accuracy of the aforementioned positioning algorithm.

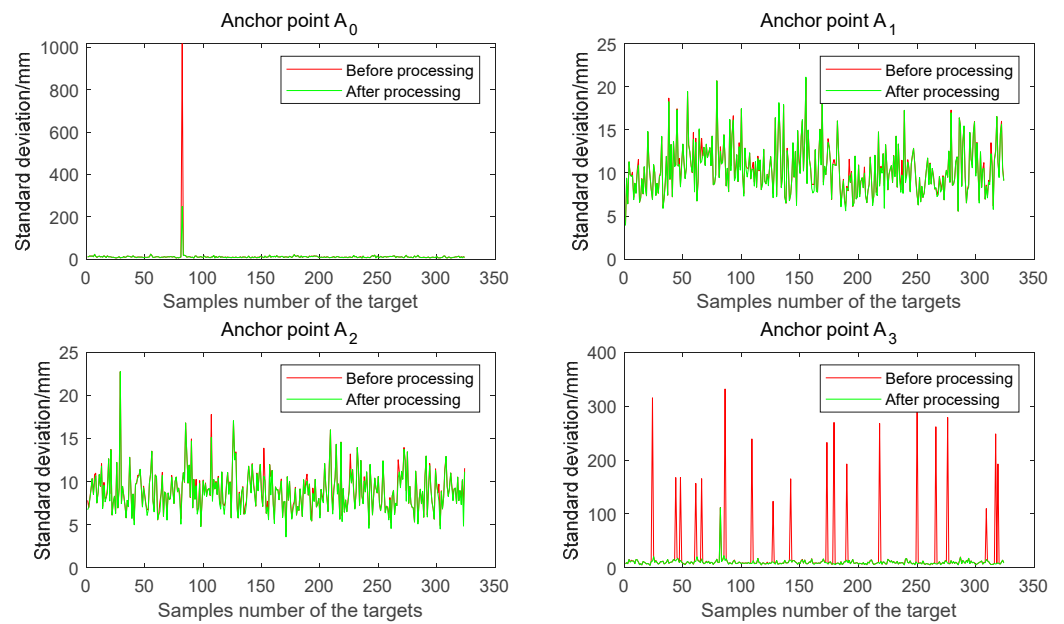


Figure 5. The standard deviation comparison of the samples before and after processing without signal interference.

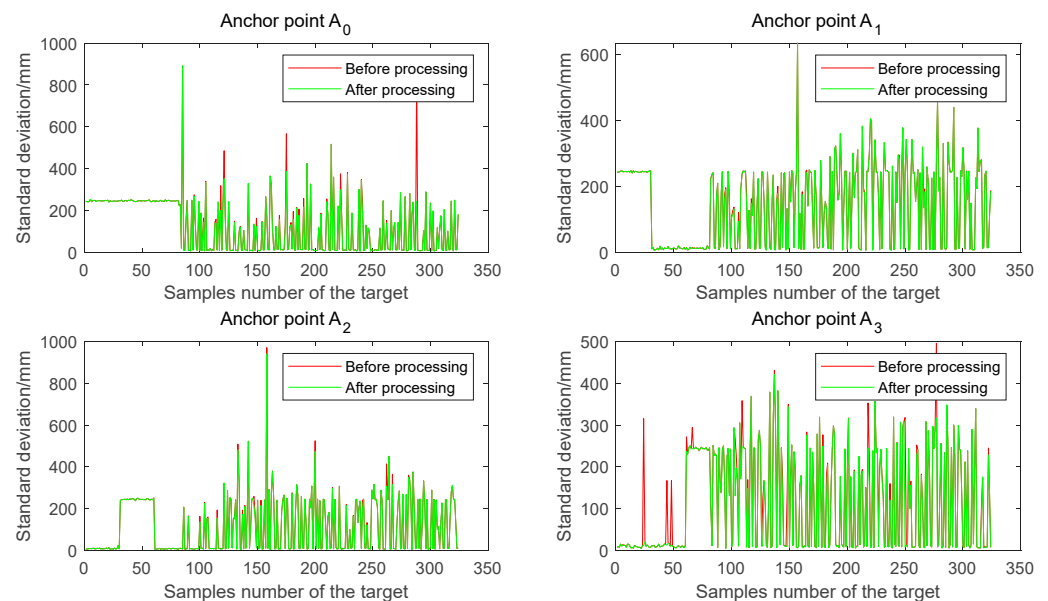


Figure 6. The standard deviation comparison of the samples before and after processing with signal interference.

4.3. Identification of Signal Interference

Firstly, these 518 samples of the training set for model training and 130 samples of the test set for model testing, were generated by the sequential shuffling method from 648 (i.e., 324×2) sets of measurement datasets. The GA-ELM model is then created and trained, and finally, the error rate of the training model is calculated and analyzed by comparison.

In the following operation, the minimum error rate of the binary classifier for judging the existence of UWB signal interference is calculated, based on GA to optimize ELM, in the activation function of Sigmoid is 3.2819%. The evolution curve is shown in Figure 7, and the comparison of the discriminant results of the test set is shown in Figure 8.

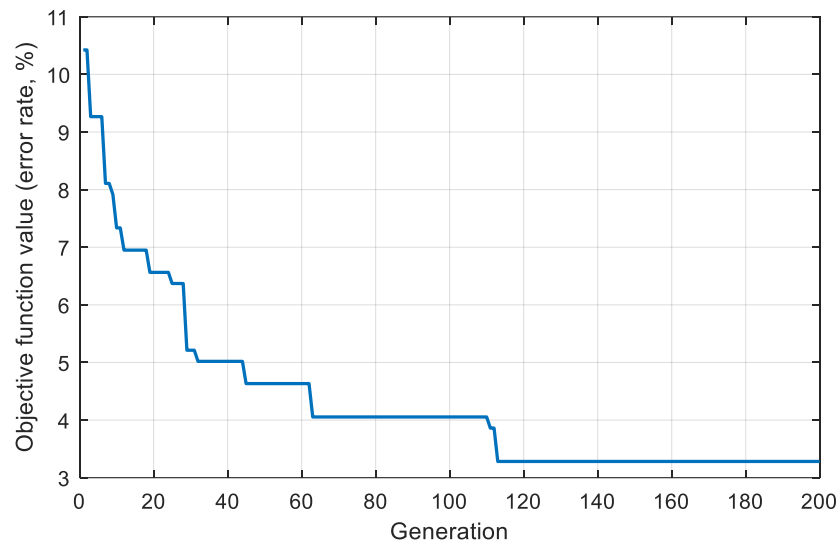


Figure 7. The evolution curve of GA-ELM classifier.

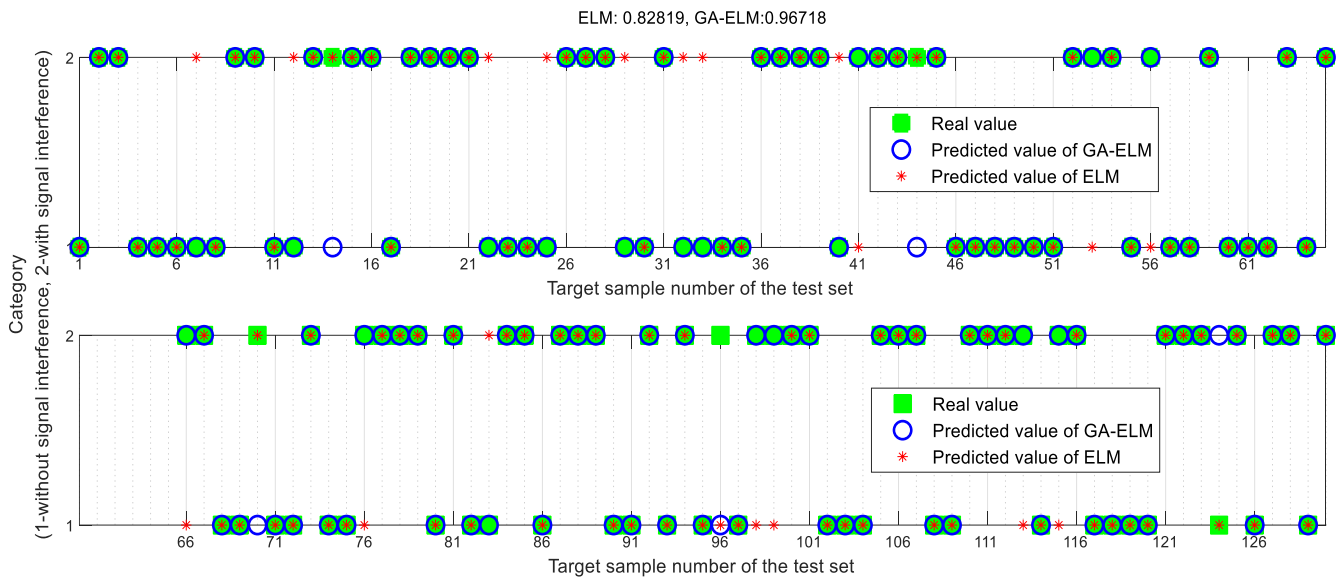


Figure 8. The comparison of the discriminant results of the test set.

In Figure 8, the numerical value on the ordinate represents the judgment of the presence and absence of signal interference. Specifically, 1 and 2 represent no signal interference and signal interference, respectively. It can be concluded that the correct rate of GA-ELM is 96.72%, which is 16.78% higher than that of ELM, manifesting that the optimization effect of GA-ELM is better than that of ELM.

More classically, support vector machine (SVM) and logistic regression (LR) can also be used as binary classifiers for signal interference discrimination. The LR model is a generalized linear regression analysis model, whose independent variables can be either continuous or categorical [51], while the SVM model is a class of generalized linear classifiers that perform binary classification of data according to supervised learning [52]. In order to further explore the superiority of the GA-optimized ELM binary classifier, the LR classifier and SVM classifier are established to compare with the GA-ELM classifier proposed in this paper, whose results of the comparison are listed in Table 2.

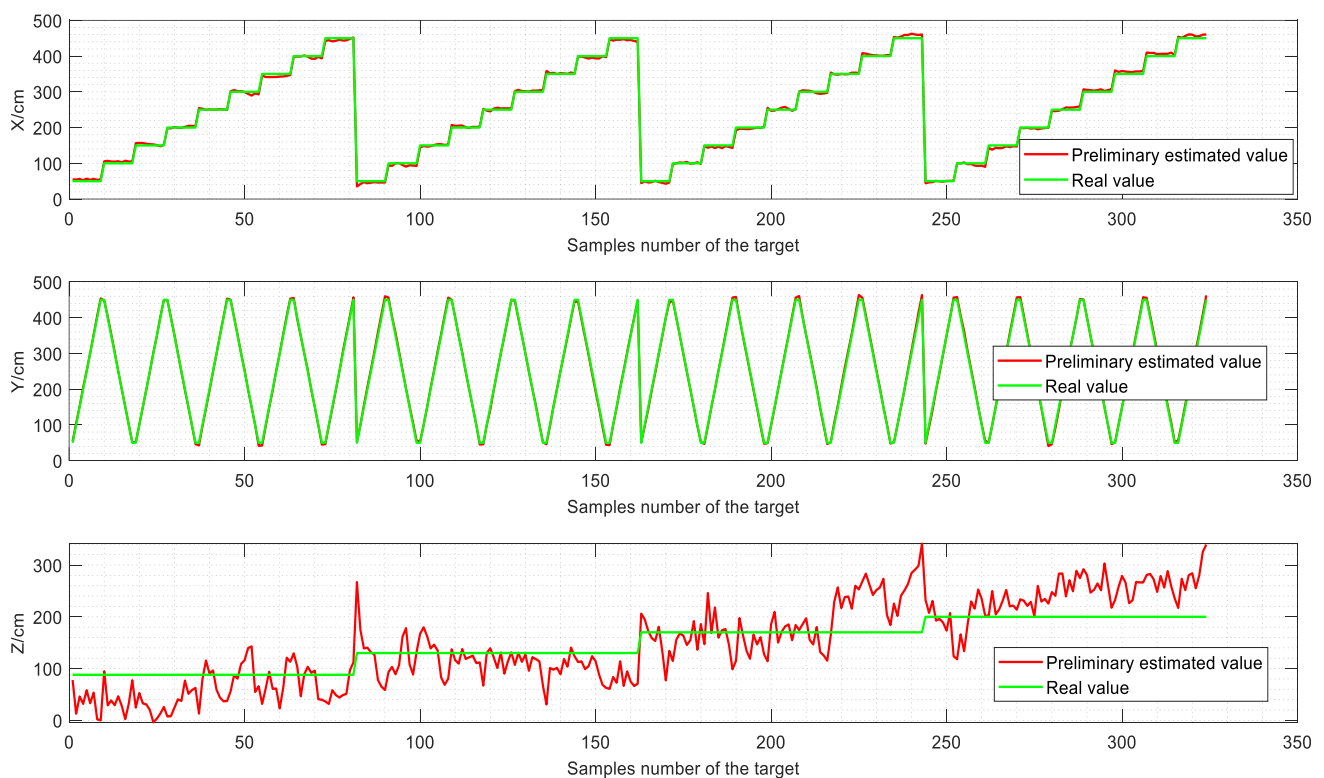
Table 2. The comparison of correct rates of different classifiers.

Serial Number	Classifier Name	Training Accuracy Rate	Test Accuracy Rate
1	LR	96.33%	63.08%
2	SVM	65.41%	56.03%
3	ELM	83.96%	82.82%
4	GA-ELM	97.92%	96.72%

By comparing these classifiers' accuracy rate of the training set and testing set, it is found that the accuracy rate of the GA-ELM classifier is the highest among these classifiers, accordingly, the GA-ELM classifier is preferred to discriminate whether the UWB signals are interfered with.

4.4. Preliminary Positioning Results and Analysis

Based on the preliminary positioning model established in Section 2, a rigorous numerical comparison chart concerning the true value and the estimated value of the target coordinates with and without signal interference are shown in Figures 9 and 10, respectively. Additionally, the RMSE of the target coordinates with and without signal interference are tabulated in Table 3.

**Figure 9.** The comparison of the true value and estimated value of the target coordinates without signal interference.

In the comparison of Figures 9 and 10 and Table 3, it is vividly depicted that errors in X and Y directions are small, only reaching centimeter-level accuracy, while errors in Z-direction are large, which reached an accuracy of the decimeter level. The reason is that the quadratic term is eliminated in Equation (5), so the target coordinates are no longer on the spherical surface with the target as the center and the measurement distance as the radius, which can potentially cause larger ranging errors. Secondly, the condition number of the coefficient matrix is much greater than one, consequently, a slight disturbance will produce a considerable error. In this case, the coordinate difference $z_i - z_{i-1}$ is one order of magnitude smaller than $x_i - x_{i-1}$ and $y_i - y_{i-1}$, which makes the errors in the Z-direction more

sensitive. Therefore, it is indispensable that the Z-axis coordinates errors compensation is carried out to accomplish accurate positioning of the target.

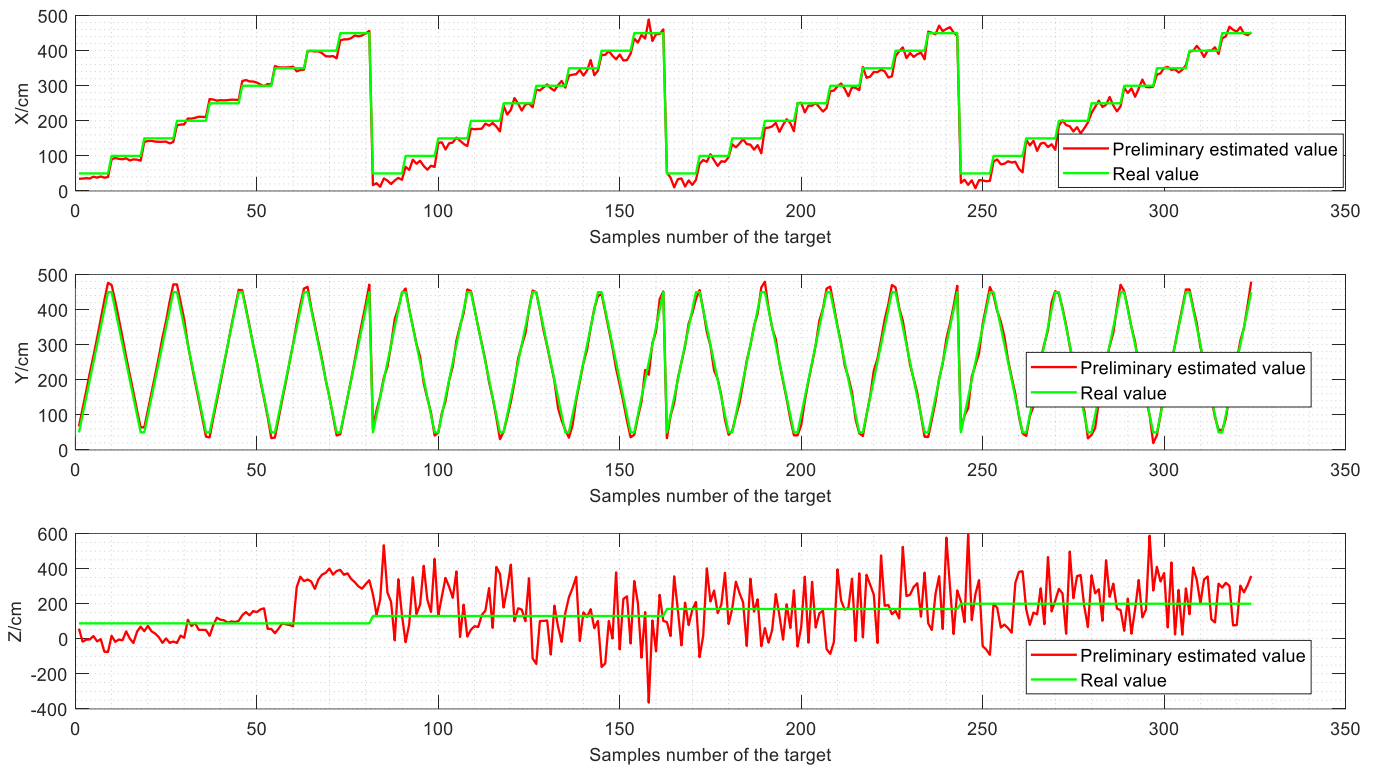


Figure 10. The comparison of the true value and estimated value of the target coordinates with signal interference.

Table 3. The RMSE of preliminary estimation of the target coordinates with and without signal interference.

The Coordinates of the Target	RMSE without Signal Interference (cm)	RMSE with Signal Interference (cm)
X	5.0187	13.5421
Y	4.6536	13.0012
Z	50.5896	148.3624
(X, Y)	6.8443	16.4087
(X, Y, Z)	51.0505	79.3578

4.5. Positioning Errors Compensation Model

The 324 groups of samples are divided into 250 training set samples and 74 test set samples. For the absence of signal interference, only the errors compensation towards the Z-axis is enough, whose training sample has four input parameters (i.e., ranging from four anchors) and one output parameter (i.e., Z-axis errors). Successively, in the case of the presence of different interfering signals, the ranging errors caused by signal interference are firstly compensated and the Z-direction errors are then compensated. The input layer and an output layer of the ranging errors compensation model each have four nodes, which are the ranging of four anchors and the ranging errors of four anchors, respectively. The following procedure is to calculate the position of the target with and without signal interference, respectively.

4.5.1. Without Signal Interference

In terms of no signal interference, the input of function expression $f : \mathbb{R}^{n \times m} \rightarrow \mathbb{R}^{n \times k}$ of the GA-optimized ELM based positioning errors compensation model is 324 groups of target position distances, each of which has distances measurement of four anchors (i.e., $n = 324, m = 4$), and the output is 324 groups Z-axis errors of the target (i.e., $k = 1$).

The GA-optimized ELM based positioning errors compensation model is applied to model training, and the minimum RMSE of the test dataset is 14.5068 cm. Then the evolution curve is shown in Figure A1, and a comparison chart of the prediction results of the Z-axis coordinate errors of the target in the test set is drawn, as shown in Figure 11. Additionally, due to the enormous number of standard and extended machine learning models used in positioning, the BP neural network is added to justify and compare the usage of the GA-ELM model for experimentation.

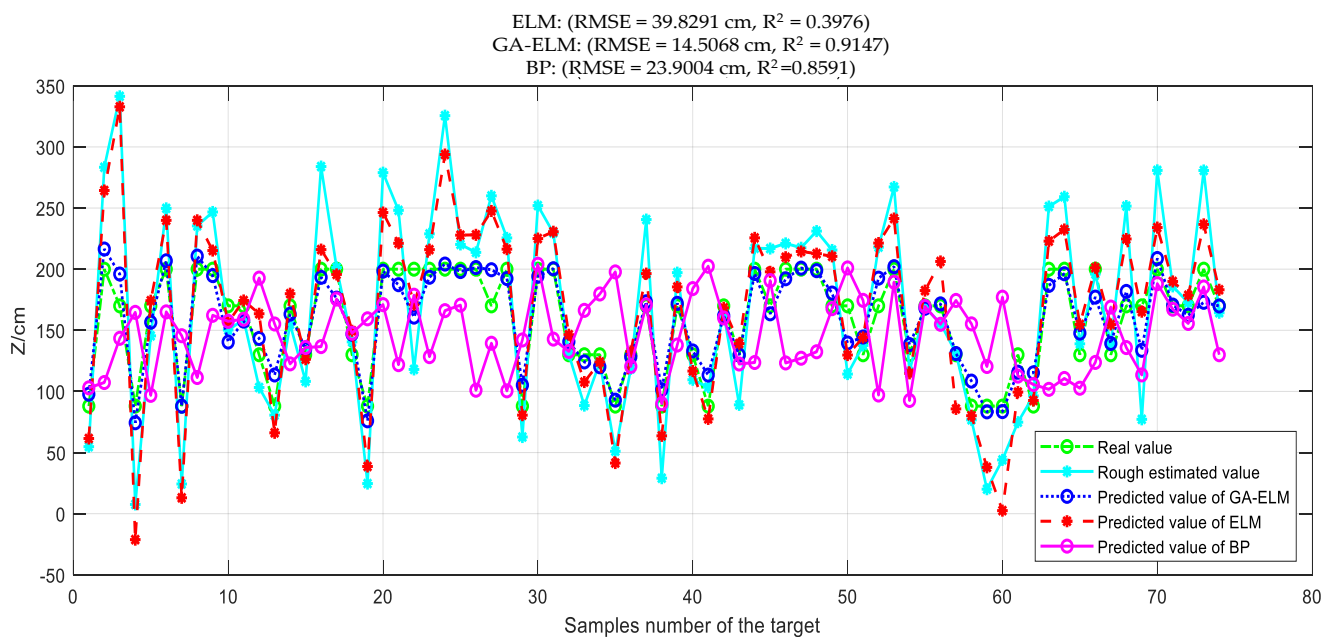


Figure 11. The comparison of the prediction results of the Z-axis errors of the test set target.

From Figure 11, it is observed that the overall effect of GA-ELM is relatively ideal, and its training set degree of fitting is 0.9147. Moreover, the minimum RMSE of GA-ELM is 14.5068 cm in the case of LOS, which is 71.32% and 59.72% less than the original estimate and the unoptimized one, respectively. Consequently, the Z-direction coordinate can be compensated according to the training prediction errors of the measurement data.

4.5.2. With Signal Interference

As for signal interference, the input of function expression $f : \mathbb{R}^{n \times m} \rightarrow \mathbb{R}^{n \times k}$ of the GA-optimized ELM, based on the ranging errors compensation model, is 324 groups of target position distances, each of which has the measured distances of four anchors (i.e., $n = 324, m = 4$), and the output is 324 ranging errors, each of which has four errors of anchors (i.e., $k = 4$). Then, the input and output of the errors compensation model for the Z-direction are the same as those without signal interference.

As detailed in Section 3, errors compensation is performed on the distances from the four anchors to the target, and the minimum of RMSE optimized by the GA-ELM model is 134.2459 cm. Then the evolution curve is shown in Figure A2, and a comparison diagram of the predicted value and the true value of the ranging errors of each anchor in the training set are shown in Figure 12.

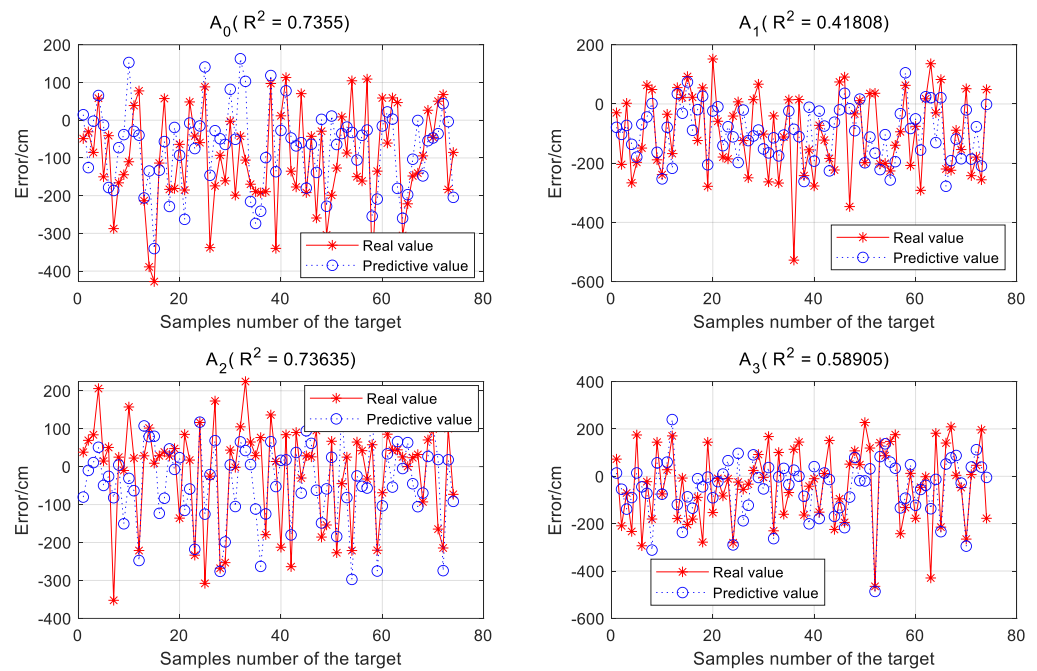


Figure 12. The comparison of ranging errors of each anchor point.

The estimated ranging errors are then substituted into the positioning model for Z-axis errors compensation, and the comparison figure before and after the compensation of range errors with signal interference is shown in Figure 13. Successively, the RMSE after errors compensation is calculated and compared with the one before compensation in Table 4.

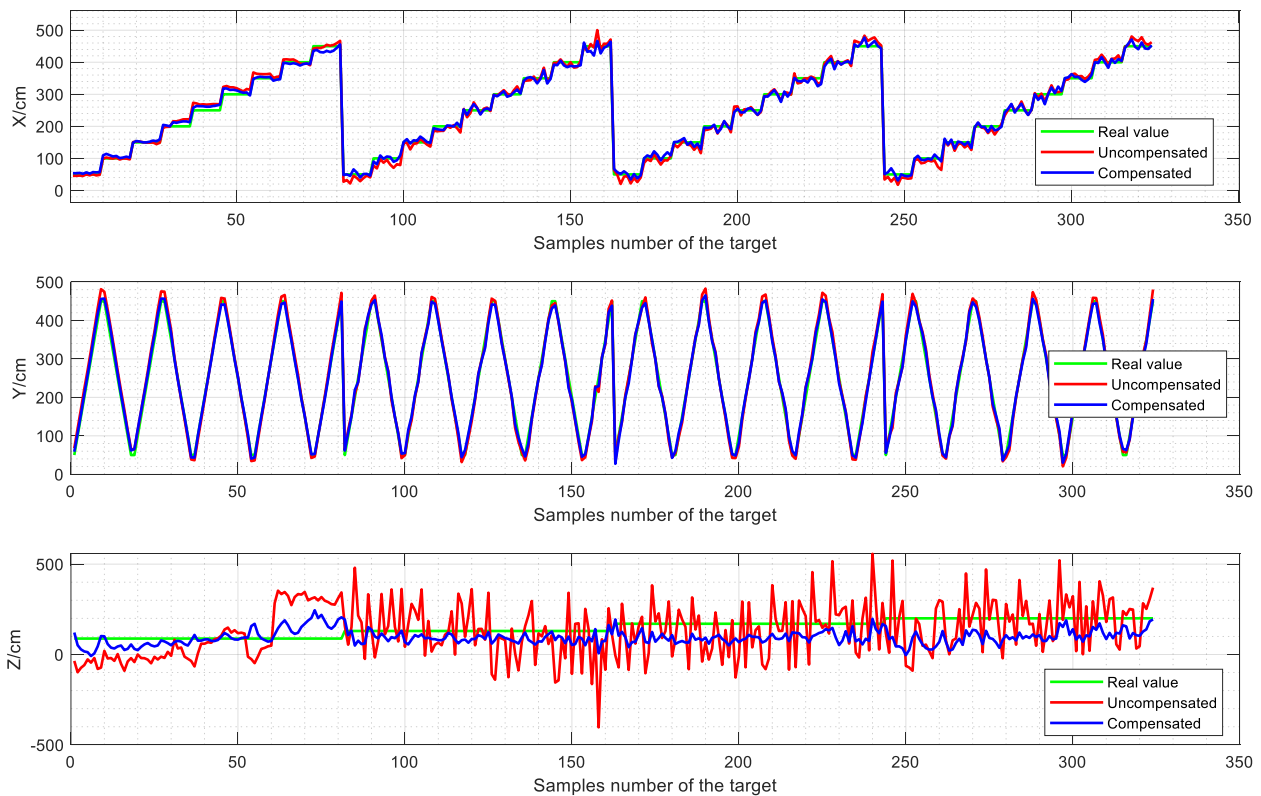


Figure 13. Comparison before and after ranging errors compensation with signal interference.

Table 4. RMSE before and after compensation of ranging errors with signal interference.

Serial Number	Target Coordinates	RMSE before Compensation (cm)	RMSE after Compensation (cm)	Reduction Percentage of RMSE
1	X	13.5421	10.1621	24.96%
2	Y	13.0012	9.2658	28.73%
3	Z	148.3624	77.6429	47.67%
4	(X, Y)	16.4087	13.7522	16.19%
5	(X, Y, Z)	79.3578	78.8514	0.64%

From the rigorous numerical comparison of Figure 13 and Table 4, it can be concluded that after the ranging errors compensation with signal interference, the RMSE of the Z-direction is reduced by nearly 50%, which shows the effectiveness of the errors compensation model. However, there is still room for improvement in the errors of the Z-axis compared with those precision free of signal interference. Therefore, compensation for the Z-axis errors is equivalent to dual errors compensation for signal interference, which can effectively improve the positioning accuracy of the three-dimensional space coordinates of the target on the mobile robot.

The Z-axis errors are compensated by using the data after ranging errors compensation, and finally, the minimum RMSE is 37.9811 cm, of which the evolution curve is shown in Figure A3. Then, as shown in Figure 14, the Z-axis errors of the target in the test with signal interference are compared with the predicted results by forming a point plot. Meanwhile, the RMSE comparison before and after errors compensation with signal interference is shown in Table 5.

ELM: (RMSE = 125.3364 cm, $R^2 = 0.2712$)
 GA-ELM: (RMSE = 37.9811 cm, $R^2 = 0.9331$)
 BP: (RMSE = 48.5180 cm, $R^2 = 0.5602$)

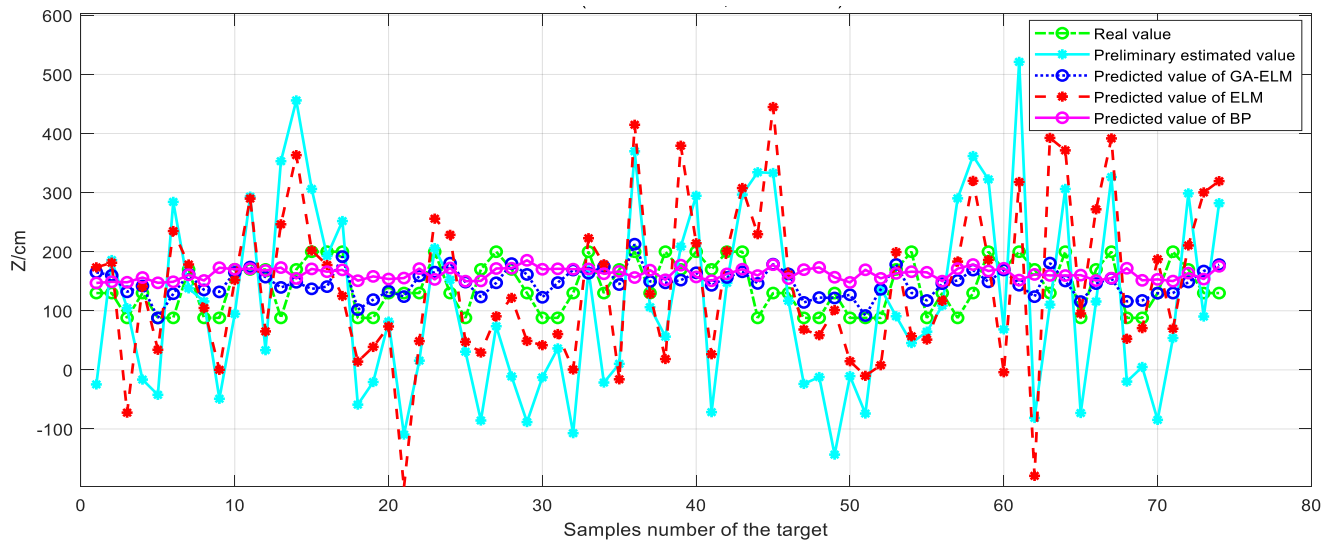


Figure 14. The comparison of Z-axis test set errors compensation with signal interference.

Table 5. RMSE before and after errors compensation with signal interference.

Serial Number	Target Coordinates	RMSE before Ranging Errors Compensation (cm)	RMSE after Ranging Errors Compensation (cm)	RMSE after Z-Axis Errors Compensation (cm)	Reduction Percentage of RMSE
1	X	13.5421	10.1621	—	24.96%
2	Y	13.0012	9.2658	—	28.73%
3	Z	148.3624	77.6429	37.9811	51.08%
4	(X, Y)	16.4087	13.7522	—	16.19%
5	(X, Y, Z)	79.3578	78.8514	28.0861	64.38%

From Table 5, it can be clearly seen that the RMSE of the spatial coordinates after compensation of the GA-ELM model is 28.0861 cm in the case of NLOS, which is 64.38% and 70.16% significantly lower than those without compensation and optimization, respectively.

In order to better compare the performance of different algorithms, it is necessary to draw a cumulative distribution function (CDF) graph of the algorithm positioning errors. Figure 15 shows the CDF comparison of different algorithms in the two cases of LOS and NLOS, where the localization errors of LOS and NLOS are uniformly distributed numbers between 0~180 cm and 0~350 cm, respectively. As can be seen from Figure 15, compared to other algorithms, the GA-ELM model performs the best with an absolute error of less than 20 cm and 50 cm at over 80% quantile, in LOS and NLOS, respectively.

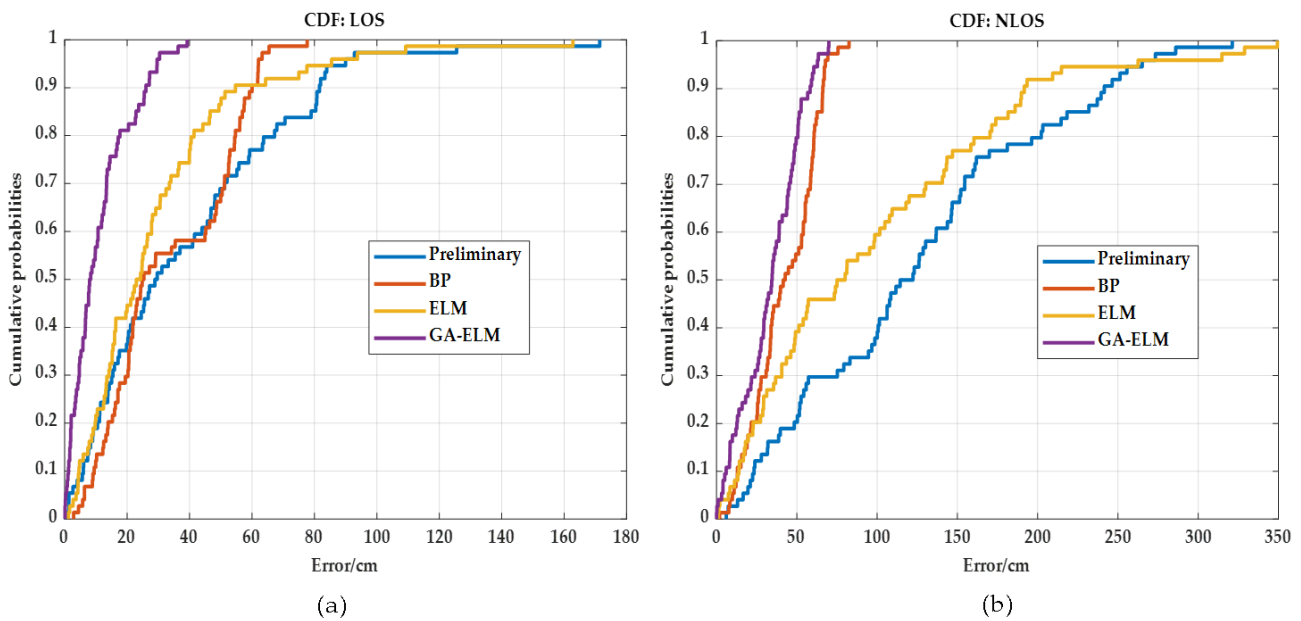


Figure 15. The comparison of CDFs for different algorithms under LOS and NLOS: (a) Without signal interference; (b) With signal interference.

In the following, the numerical results of state-of-the-art approaches provided by other researchers in comparison with the GA-ELM model proposed in this paper are summarized in Table 6. The numerical results in Table 6 demonstrate that the method proposed in this paper has high accuracy in comparison with other methods.

Table 6. The comparison of the positioning accuracy of different methods.

Number	Technology	Environment	RMSE
1	Proposed (GA-ELM, only UWB)	5 × 5 × 3 m	0.145 m (3D)
2	Zigbee [9]	4 × 4 m	0.636 m (2D)
3	LiDAR, SRD-LS [32]	20 × 20 m	0.35 m (2D)
4	GA-RBF, UWB [43]	14 × 12 m	0.10 m (2D)
5	UWB and PDR [41]	8.5 × 4.5 m	0.51 m (2D)
6	UWB with differential evolution [48]	15 × 10 m	0.56 m (2D)
7	UWB with monocular simultaneous [19]	6 × 6 × 4.5 m	0.139 m (3D)
8	UWB, IMU, multiple onboard visual-inertial and lidar odometry subsystems [36]	6 × 4 × 3 m	0.33 m (3D)

Finally, as depicted in Figure 16, the target positioning trajectory is connected into a smooth transition three-dimensional curve by denoising the trajectory of the mobile robot, and views of XOZ and XOY are drawn to make the trajectory of the target in the Z-axis more clearly expressed.

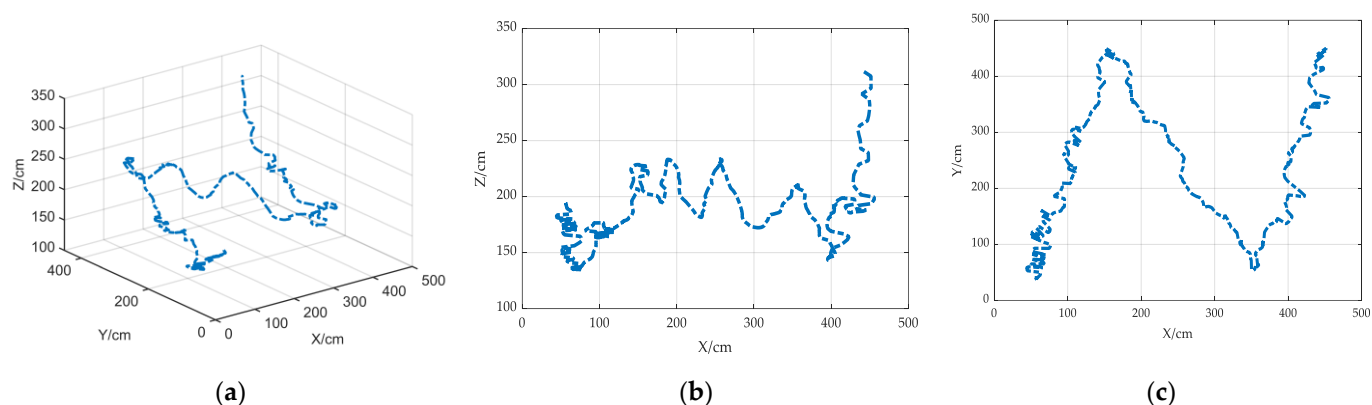


Figure 16. Trajectory of the target: (a) View of three-dimensional; (b) View of XOZ; (c) View of XOY.

5. Conclusions

This study presents an improved extreme learning machine based UWB positioning for mobile robots with signal interference. It is worth mentioning that the implementation costs of this proposed method are comparably low since only UWB technology is used instead of extra hardware, as compared to solutions (provided by other researchers) of multi-sensor fusion with high costs. The main contributions of the work can be summarized as follows:

1. By combining the advantages of ELM and GA, the GA-optimized ELM model, for optimizing the weight coefficients and thresholds of ELM by GA, is constructed, which can achieve both classification (discrete) and prediction (continuous).
2. A binary classifier for the signal interference discrimination and positioning errors compensation model, based on the GA-optimized ELM model mentioned above, is proposed so as to judge whether the UWB signals are disturbed and compensate for the positioning errors, respectively.
3. This proposed model was tested on 628 available datasets of actual scene experiments, and it is concluded from the comparison of results that the minimum RMSE with signal interference reduced dramatically (64.38% and 70.16%), which means improvement of accuracy compared with those results free of compensation and optimization. The position of mobile robots can be calculated with decimeter-level accuracy, even in complicated indoor environments.

In the future work as an extension of this, an improved model able to identify which anchor signals are interfered with and thus, cause positioning errors will be developed, and the potential impact of robot mobility and increase in the speed of the positioning accuracy for the mobile robot will be thoroughly considered.

Author Contributions: Conceptualization, X.D. and J.M.; methodology, J.M. and X.D.; software, J.M.; validation, X.D. and D.Z.; formal analysis, X.D.; investigation, C.S.; resources, X.D.; data curation, M.M.; writing—original draft preparation, J.M.; writing—review and editing, X.D., C.S. and M.M.; visualization, J.M.; supervision, X.D.; project administration, J.M.; funding acquisition, X.D. All authors have read and agreed to the published version of the manuscript.

Funding: This research was supported by Natural Science Basic Research Plan in Shaanxi Province of China under Grant 2021JM-122.

Institutional Review Board Statement: Not applicable.

Informed Consent Statement: Not applicable.

Data Availability Statement: Not applicable.

Acknowledgments: Thanks to the National 111 Project Base for Electronic Equipment Electromechanical Coupling Theory and Technology.

Conflicts of Interest: The authors declare no conflict of interest.

Appendix A

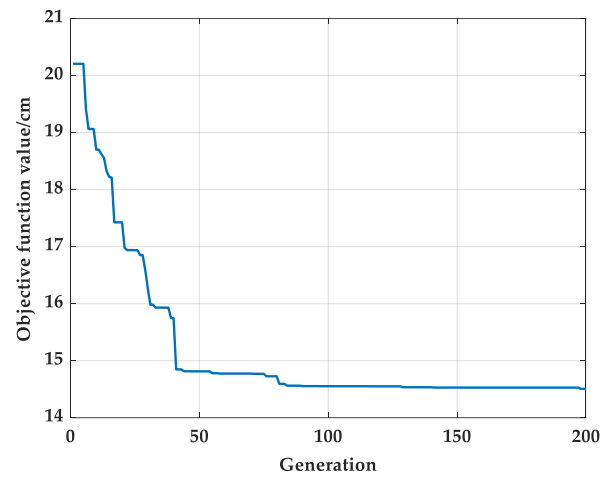


Figure A1. Errors evolution curve without signal interference.

Appendix B

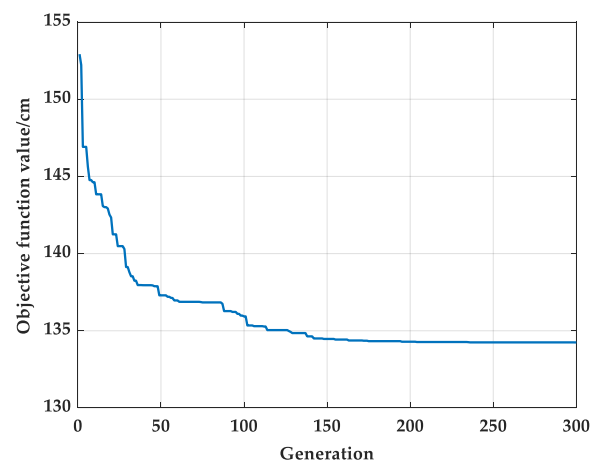


Figure A2. The evolution curve of ranging errors with signal interference.

Appendix C

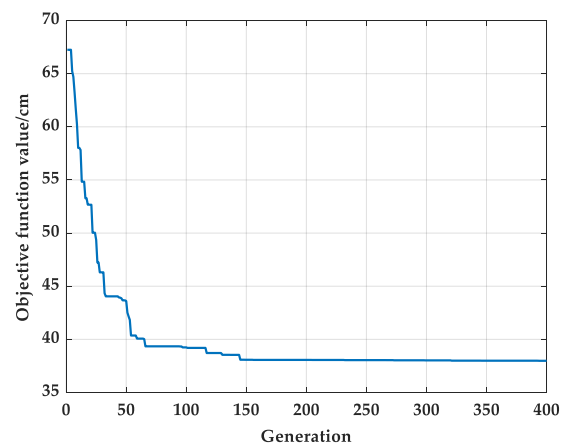


Figure A3. The evolution curve of Z-axis errors compensation with signal interference.

References

1. Zhao, L.; He, Z. An in-coordinate interval adaptive Kalman filtering algorithm for INS/GPS/SMNS. In Proceedings of the IEEE 10th International Conference on Industrial Informatics, Beijing, China, 25–27 July 2012; pp. 41–44.
2. Ulusar, U.D.; Celik, G.; Al-Turjman, F. Cognitive RF-based localization for mission-critical applications in smart cities: An overview. *Comput. Electr. Eng.* **2020**, *87*, 106780. [[CrossRef](#)]
3. Khan, D.; Ullah, S.; Nabi, S. A Generic Approach toward Indoor Navigation and Pathfinding with Robust Marker Tracking. *Remote Sens.* **2019**, *11*, 3052. [[CrossRef](#)]
4. Wang, Y.; Guan, W.; Hussain, B.; Yue, C.P. High Precision Indoor Robot Localization Using VLC Enabled Smart Lighting. In Proceedings of the Optical Fiber Communication Conference (OFC) 2021, Washington, DC, USA, 6–11 June 2021; p. M1B.8.
5. Ashraf, I.; Hur, S.; Park, Y. Indoor Positioning on Disparate Commercial Smartphones Using Wi-Fi Access Points Coverage Area. *Sensors* **2019**, *19*, 4351. [[CrossRef](#)]
6. Ashraf, I.; Hur, S.; Park, Y. Enhancing Performance of Magnetic Field Based Indoor Localization Using Magnetic Patterns from Multiple Smartphones. *Sensors* **2020**, *20*, 2704. [[CrossRef](#)]
7. Ashraf, I.; Hur, S.; Shafiq, M.; Kumari, S.; Park, Y. GUIDE: Smartphone sensors-based pedestrian indoor localization with heterogeneous devices. *Int. J. Commun. Syst.* **2019**, *32*, e4062. [[CrossRef](#)]
8. Gomes, E.L.; Fonseca, M.; Lazzaretti, A.E.; Munaretto, A.; Guerber, C. Clustering and Hierarchical Classification for High-Precision RFID Indoor Location Systems. *IEEE Sens J.* **2021**, in press.
9. Zhang, L.; Zhang, S.; Leng, C.T. A Study on the Location System Based on Zigbee for Mobile Robot. *Appl. Mech. Mater.* **2014**, *651*, 612–615. [[CrossRef](#)]
10. Liu, G.; Qian, Z.; Wang, X. An Indoor WLAN Location Algorithm Based on Fingerprint Database Processing. *Intern. J. Pattern Recognit. Artif. Intell.* **2020**, *34*, 2050026. [[CrossRef](#)]
11. Zhang, L.; Meng, X.; Fang, C. Linear Regression Algorithm against Device Diversity for the WLAN Indoor Localization System. *Wirel. Commun. Mob. Comput.* **2021**, *2021*, 5530396. [[CrossRef](#)]
12. Cazzorla, A.; Angelis, D.G.; Moschitta, A.; Dionigi, M.; Alimenti, F.; Carbone, P. A 5.6-GHz UWB Position Measurement System. *IEEE Trans. Instrum. Meas.* **2013**, *62*, 675–683. [[CrossRef](#)]
13. Marandò, S.; Gifford, W.M.; Wymeersch, H.; Win, M.Z. NLOS identification and mitigation for localization based on UWB experimental data. *IEEE J. Sel. Areas Commun.* **2010**, *28*, 1026–1035. [[CrossRef](#)]
14. Yu, X.; Li, Q.; Queralta, J.P.; Heikkonen, J.; Westerlund, T. Applications of UWB Networks and Positioning to Autonomous Robots and Industrial Systems. In Proceedings of the 2021 10th Mediterranean Conference on Embedded Computing (MECO), Budva, Montenegro, 7–10 June 2021; pp. 1–6.
15. Queralta, J.P.; Martínez Almansa, C.; Schiano, F.; Floreano, D.; Westerlund, T. UWB-based System for UAV Localization in GNSS-Denied Environments: Characterization and Dataset. In Proceedings of the 2020 IEEE/RSJ International Conference on Intelligent Robots and Systems (IROS), Las Vegas, NV, USA, 24 October–24 January 2021; pp. 4521–4528.
16. Schmid, L.; Salido-Monzú, D.; Wieser, A. Accuracy Assessment and Learned Error Mitigation of UWB ToF Ranging. In Proceedings of the 2019 International Conference on Indoor Positioning and Indoor Navigation (IPIN), Pisa, Italy, 30 September–3 October 2019; pp. 1–8.
17. Oguntala, G.; Abd-Alhameed, R.; Jones, S.; Noras, J.; Patwary, M.; Rodriguez, J. Indoor location identification technologies for real-time IoT-based applications: An inclusive survey. *Comput. Sci. Rev.* **2018**, *30*, 55–79. [[CrossRef](#)]
18. Mortier, J.; Pagès, G.; Vilà-Valls, J. Robust TOA-Based UAS Navigation under Model Mismatch in GNSS-Denied Harsh Environments. *Remote Sens.* **2020**, *12*, 2928. [[CrossRef](#)]
19. Tiemann, J.; Ramsey, A.; Wietfeld, C. Enhanced UAV Indoor Navigation through SLAM-Augmented UWB Localization. In Proceedings of the 2018 IEEE International Conference on Communications Workshops (ICC Workshops), Kansas City, MO, USA, 20–24 May 2018; pp. 1–6.
20. Khawaja, W.; Ozdemir, O.; Erden, F.; Guvenc, I.; Matolak, D.W. Ultra-Wideband Air-to-Ground Propagation Channel Characterization in an Open Area. *IEEE Trans. Aerosp. Electron. Syst.* **2020**, *56*, 4533–4555. [[CrossRef](#)]
21. Xu, H.; Wang, L.; Zhang, Y.; Qiu, K.; Shen, S. Decentralized Visual-Inertial-UWB Fusion for Relative State Estimation of Aerial Swarm. In Proceedings of the 2020 IEEE International Conference on Robotics and Automation (ICRA), Paris, France, 31 May–31 August 2020; pp. 8776–8782.
22. Corrales, J.A.; Candelas, F.A.; Torres, F. Hybrid tracking of human operators using IMU/UWB data fusion by a Kalman filter. In Proceedings of the 2008 3rd ACM/IEEE International Conference on Human-Robot Interaction (HRI), Amsterdam, The Netherlands, 12–15 March 2008; pp. 193–200.
23. Waqar, A.; Ahmad, I.; Habibi, D.; Phung, Q.C. Analysis of GPS and UWB positioning system for athlete tracking. *Meas. Sens.* **2021**, *14*, 100036. [[CrossRef](#)]
24. Monica, S.; Ferrari, G. Robust UWB-Based Localization with Application to Automated Guided Vehicles. *Adv. Intell. Syst.* **2021**, *3*, 2000083. [[CrossRef](#)]
25. De Angelis, G.; Baruffa, G.; Cacopardi, S. GNSS/cellular hybrid positioning system for mobile users in urban scenarios. *IEEE Trans. Intell. Transp. Syst.* **2013**, *14*, 313–321. [[CrossRef](#)]
26. Masiero, A.; Toth, C.; Gabela, J.; Retscher, G.; Kealy, A.; Perakis, H.; Gikas, V.; Grejner-Brzezinska, D. Experimental Assessment of UWB and Vision-Based Car Cooperative Positioning System. *Remote Sens.* **2021**, *13*, 4858. [[CrossRef](#)]

27. Hämäläinen, M.; Mucchi, L.; Caputo, S.; Biotti, L.; Ciani, L.; Marabissi, D.; Patrizi, G. Ultra-Wideband Radar-Based Indoor Activity Monitoring for Elderly Care. *Sensors* **2021**, *21*, 3158. [[CrossRef](#)]
28. Lu, C.L.; Liu, Z.Y.; Huang, J.T.; Huang, C.I.; Wang, B.H.; Chen, Y.; Wu, N.H.; Wang, H.C.; Giarré, L.; Kuo, P.Y. Assistive Navigation Using Deep Reinforcement Learning Guiding Robot With UWB/Voice Beacons and Semantic Feedbacks for Blind and Visually Impaired People. *Front. Robot. AI* **2021**, *8*, 654132. [[CrossRef](#)] [[PubMed](#)]
29. Wu, P.; Wen, D.L. Positioning Information System of Indoor Food Delivery Robot Based on UWB. *J. Phys. Conf. Ser.* **2021**, *1732*, 012129. [[CrossRef](#)]
30. Barral, V.; Escudero, C.J.; García-Naya, J.A.; Maneiro-Catoira, R. NLOS Identification and Mitigation Using Low-Cost UWB Devices. *Sensors* **2019**, *19*, 3464. [[CrossRef](#)]
31. Djosic, S.; Stojanovic, I.; Jovanovic, M.; Nikolic, T.; Djordjevic, G.L. Fingerprinting-assisted UWB-based localization technique for complex indoor environments. *Expert Syst. Appl.* **2021**, *167*, 114188. [[CrossRef](#)]
32. Pınar, O.E. TDOA based localization and its application to the initialization of LiDAR based autonomous robots. *Rob. Auton. Syst.* **2020**, *131*, 103590.
33. Zhang, S.L.; Tan, X.Q.; Wu, Q.W. Indoor mobile robot localization based on multi-sensor fusion technology. *Transducer Microsyst. Technol.* **2021**, *40*, 53–56.
34. Song, Y.; Guan, M.; Tay, W.P.; Law, C.L.; Wen, C. UWB/LiDAR Fusion for Cooperative Range-Only SLAM. In Proceedings of the 2019 International Conference on Robotics and Automation (ICRA), Montreal, QC, Canada, 20–24 May 2019; pp. 6568–6574.
35. Jorge, P.Q.; Li, Q.Q.; Fabrizio, S.; Tomi, W. VIO-UWB-Based Collaborative Localization and Dense Scene Reconstruction within Heterogeneous Multi-Robot Systems. *arXiv* **2020**, arXiv:2011.00830.
36. Nguyen, T.M.; Cao, M.; Yuan, S.; Lyu, Y.; Nguyen, T.H.; Xie, L. VIRAL-Fusion: A Visual-Inertial-Ranging-Lidar Sensor Fusion Approach. *IEEE Trans. Robot.* **2021**, *accepted*.
37. Nguyen, V.D.; Soh, G.S.; Foong, S.; Wood, K. Localization of a Miniature Spherical Rolling Robot Using IMU, Odometry and UWB. In Proceedings of the ASME 2018 International Design Engineering Technical Conferences and Computers and Information in Engineering Conference, Quebec City, QC, Canada, 26–29 August 2018; Volume 5A.
38. Sun, Y. Autonomous Integrity Monitoring for Relative Navigation of Multiple Unmanned Aerial Vehicles. *Remote Sens.* **2021**, *13*, 1483. [[CrossRef](#)]
39. Fernando, E.; Mann, G.K.; De Silva, O.; Gosine, R.G. Design and Analysis of a Pose Estimator for Quadrotor MAVs With Modified Dynamics and Range Measurements. In Proceedings of the ASME 2017 Dynamic Systems and Control Conference, Tysons, VA, USA, 11–13 October 2017; p. V003T39A008.
40. Liu, R.; Yuen, C.; Do, T.; Jiao, D.; Liu, X.; Tan, U. Cooperative relative positioning of mobile users by fusing IMU inertial and UWB ranging information. In Proceedings of the 2017 IEEE International Conference on Robotics and Automation (ICRA), Singapore, 29 May–3 June 2017; pp. 5623–5629.
41. Chen, P.; Kuang, Y.; Chen, X. A UWB/Improved PDR Integration Algorithm Applied to Dynamic Indoor Positioning for Pedestrians. *Sensors* **2017**, *17*, 2065. [[CrossRef](#)]
42. De Angelis, G.; Moschitta, A.; Carbone, P. Positioning Techniques in Indoor Environments Based on Stochastic Modeling of UWB Round-Trip-Time Measurements. *IEEE Trans. Intell. Transp. Syst.* **2016**, *17*, 2272–2281. [[CrossRef](#)]
43. Guo, H.; Li, M. Indoor Positioning Optimization Based on Genetic Algorithm and RBF Neural Network. In Proceedings of the 2020 IEEE International Conference on Power, Intelligent Computing and Systems (ICPICS), Shenyang, China, 28–30 July 2020; pp. 778–781.
44. Guo, H.; Li, M.Q.; Zhang, X.J.; Liu, Q.; Gao, X.T. Research on Indoor Wireless Positioning Precision Optimization Based on UWB. *J. Web Eng.* **2020**, *19*, 1017–1048. [[CrossRef](#)]
45. Nguyen, D.T.; Lee, H.G.; Jeong, E.R.; Lee, H.L.; Joung, J. Deep Learning-Based Localization for UWB Systems. *Electronics* **2020**, *9*, 1712. [[CrossRef](#)]
46. Nilwong, S.; Hossain, D.; Kaneko, S.-i.; Capi, G. Deep Learning-Based Landmark Detection for Mobile Robot Outdoor Localization. *Machines* **2019**, *7*, 25. [[CrossRef](#)]
47. Rana, S.P.; Dey, M.; Siddiqui, H.U.; Tiberi, G.; Ghavami, M.; Dudley, S. UWB localization employing supervised learning method. In Proceedings of the 2017 IEEE 17th International Conference on Ubiquitous Wireless Broadband (ICUWB), Salamanca, Spain, 12–15 September 2017; pp. 1–5.
48. Pan, H.; Qi, X.G.; Liu, M.L.; Liu, L.F. Map-aided and UWB-based anchor placement method in indoor localization. *Neural. Comput. Appl.* **2021**, *33*, 11845–11859. [[CrossRef](#)]
49. Huang, G.B.; Zhu, Q.Y.; Siew, C.K. Extreme learning machine: Theory and applications. *Neurocomputing* **2006**, *70*, 489–501. [[CrossRef](#)]
50. Huang, Z.; Wu, W.; Liu, H.; Zhang, W.; Hu, J. Identifying Dynamic Changes in Water Surface Using Sentinel-1 Data Based on Genetic Algorithm and Machine Learning Techniques. *Remote Sens.* **2021**, *13*, 3745. [[CrossRef](#)]
51. Zou, X.; Hu, Y.; Tian, Z.; Shen, K. Logistic Regression Model Optimization and Case Analysis. In Proceedings of the 2019 IEEE 7th International Conference on Computer Science and Network Technology (ICCSNT), Dalian, China, 19–20 October 2019; pp. 135–139.
52. Borges, F.; Pinto, A.; Ribeiro, D.; Barbosa, T.; Pereira, D.; Magalhães, R.; Barbosa, B.; Ferreira, D. An Unsupervised Method based on Support Vector Machines and Higher-Order Statistics for Mechanical Faults Detection. *IEEE Lat. Am. Trans.* **2020**, *18*, 1093–1101. [[CrossRef](#)]